

Networking Low-Power Energy Harvesting Devices: Measurements and Algorithms

Maria Gorlatova*, Aya Wallwater†, Gil Zussman*

*Electrical Engineering, †Industrial Engineering and Operations Research

Columbia University, New York, NY, 10027

Email: {mag2206, aw2589}@columbia.edu, gil@ee.columbia.edu

Abstract—Recent advances in energy harvesting materials and ultra-low-power communications will soon enable the realization of networks composed of energy harvesting devices. These devices will operate using very low ambient energy, such as indoor light energy. We focus on characterizing the energy availability in indoor environments and on developing simple rate allocation algorithms that can be implemented in ultra-low-power devices. First, we present results of our *long-term indoor radiant energy measurement campaign*, which provide important inputs required for algorithm and system design (e.g., determining the required battery sizes). Then, we focus on algorithm development, which requires non-traditional approaches, since energy harvesting shifts the nature of energy-aware protocols *from minimizing energy expenditure to optimizing it*. Moreover, in many cases, different energy storage types (rechargeable battery and a capacitor) require different algorithmic treatment. In particular, we develop algorithms for determining the energy spending rates in systems with *predictable* energy inputs. Then, we focus on the spending rate control problem in systems with *stochastic* energy inputs. Finally, we utilize our measurements to present numerical results that demonstrate the operation of the different algorithms.

Index Terms—Energy harvesting, ultra-low-power networking, indoor radiant energy, measurements, energy-aware algorithms.

I. INTRODUCTION

Recent advances in the areas of solar, piezoelectric, and thermal energy harvesting [39], and in ultra-low-power wireless communications [47] will soon enable the realization of perpetual *energy harvesting wireless devices*. When networked together, they can compose rechargeable sensor networks [28], [40], [45], [51], networks of computational RFIDs [23], and Energy Harvesting Active Networked Tags (EnHANTs) [20], [21]. Such networks will find applications in various areas, and therefore, the wireless industry is already engaged in the design of various devices (e.g., [2], [9]).

In this paper we focus on devices that harvest *ambient light energy*. Since there are 3 orders of magnitude between light energy available indoor and outdoor [21], [41], significantly different algorithms are required for different environments. However, there is lack of data and analysis regarding the energy availability in such environments. Hence, over the past year we have been performing a first-of-its-kind measurement campaign that enables *characterizing the energy available in indoor environments*. We describe the results and show that they provide insights that can be used for the development of energy-harvesting-aware algorithms and systems.

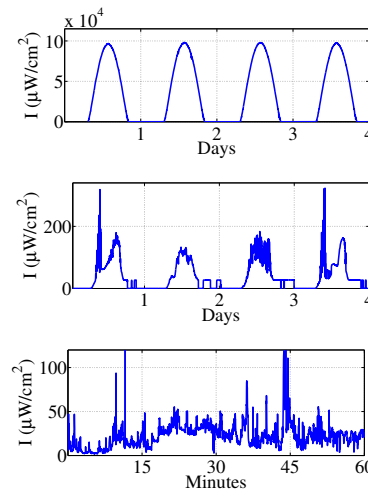


Fig. 1. Examples of different radiant (light) energy sources: (top) *Predictable profile* (Las Vegas, NV [5], outdoors), (middle) *Partially-predictable profile* (New York, NY, a static indoor device), and (bottom) *Stochastic behavior* (New York, NY, a mobile device in Times Square at nighttime).

Clearly, there has been an extensive research effort in the area of energy efficient algorithms for sensor networks and for wireless networks in general. However, for devices with renewable energy sources, fundamentally different problems arise. Hence, in the second part of the paper we focus on developing simple algorithms for determining the energy spending rates and the data rates in various scenarios.

To describe our contributions, we introduce below several dimensions of the algorithm design space. The combinations of parameters along these dimensions induce “working points”, some of which have been studied recently (see Section II).

- **Environmental energy model:** predictable and partially-predictable energy profile, stochastic process, model-free.
- **Energy storage type:** battery, capacitor.
- **Ratio of energy storage capacity to energy harvested:** large to small.
- **Time granularity:** sub-seconds to days.
- **Problem size:** stand-alone node, node pair (link), cluster, multihop network.

A. Environmental Energy Models

The model representing harvested energy depends on various parameters such as the energy source (i.e., solar, kinetic,

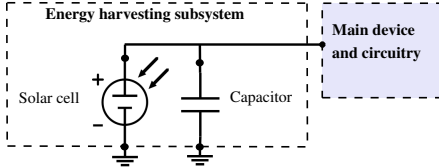


Fig. 2. A schematic representation of a capacitor-based radiant energy harvesting system.

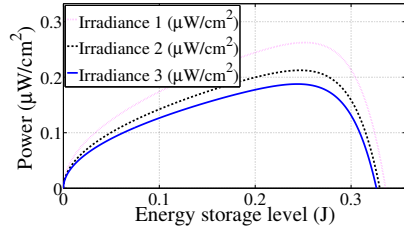


Fig. 3. An example of power vs. storage curves for a capacitor-based radiant energy harvesting system.

thermal), the properties of the environment, and the device’s behavior (stationary, semi-stationary, or mobile). Fig. 1 provides examples of radiant (light) energy sources in different settings. In Fig. 1(a) the energy availability is time-dependent and predictable, while in Fig. 1(b) that corresponds to an indoor environment, it is time-dependent and periodic, but harder to predict. Time-dependent and somewhat periodic behaviors (along with inputs such as weather forecasts) would allow to develop an *energy profile* [15], [29]. We will refer to ideal energy profiles that accurately represent the future as *predictable profiles*, and to those that are not accurate as *partially-predictable profiles*.

Energy behavior that does not warrant a time-dependent profile appears in Fig. 1(c), which shows the irradiance recorded by a *mobile device* carried around Times Square at *nighttime*. In this case, the energy can be modeled by a *stochastic process*. Other scenarios where stochastic models are a good fit are a floorboard that gathers energy when stepped on and a solar cell in a room where lights go on and off as people enter and leave. Finally, in some settings not relying on a particular model of energy (*model-free approach*) is most suitable.

B. Energy Storage Types

Without storing energy, a device can operate only when directly powered by environmental energy. Energy harvesting systems can rely on *rechargeable batteries* or *capacitors* for storage. *Batteries* can be modeled by an ideal (linear) model, where the changes in the amount of stored energy are linearly related to the amounts of energy harvested or spent, or more realistically by considering their chemical characteristics [42]. Use of *capacitors* as the energy storage has only recently started gaining attention [23], [28], [51].

We consider an important aspect of capacitor-based systems. Due to the *highly non-linear output versus voltage characteristics*, in a simple capacitor-based system, the amount of energy harvested depends both on the amount of energy provided, and on *the amount of energy stored* [23], [35]. The non-linear

relations are demonstrated in Fig. 3.

C. Storage Capacity, Decision Timescale, and Problem Size

Storage capacity vs. amount of energy harvested – Energy storage capacity can be 4700 J for an AA battery and 0.16J for an EnerChips ‘battery in a chip’ system [2]. The available energy also differs widely, and can be as high as thousands of $J/cm^2/day$ in sunny outdoor environments and as low as under $2 J/cm^2/day$ in indoor environments (see section IV). Different combinations require different algorithmic approaches. For example, when the storage is small compared to the rate, the algorithms must continuously keep track of the energy levels, to guarantee that the storage is not depleted or that recharging opportunities are missed. On the other hand, with relatively large storage, simpler algorithms can be used.

Time granularity – Nodes can characterize the received energy and make decisions on timescales from seconds to days. This timescale is related to the storage-harvesting ratio and the environmental energy model.

Problem/Network Size – Energy harvesting affects nodes’ individual decisions, pairwise (link) decisions, and behavior of networked nodes (e.g., routing and rate adaptation).

D. Our Contributions

First, we present the results of a *year-long indoor and mobile outdoor radiant energy measurements campaign* that provide important input to the design of algorithms. In particular, we discuss the energy available in various indoor environments and the corresponding data rates. We also show that in indoor environments the energy models are mostly partially-predictable and that simple parameters can significantly improve predictions when the time granularity is at the order of days. To the best of our knowledge, this work is the first to present long-term indoor radiant energy measurements (the traces will be made available in CRAWDAD).

Second, we consider *predictable energy profiles* and focus on the simple cases of a *single node and a link*. Our objective is *fair allocation of resources along the time axis* which has strong ties to *economic consumption smoothing*. In particular, we use the lexicographic maximization and utility maximization frameworks to obtain the energy spending rates of a node and the data rates for a pair of nodes. We develop simple algorithms (that can be implemented in resource constrained nodes) both for a battery-based system and for a *capacitor-based system* and consider the *ratios between harvesting rate and storage size*. In particular, to the best of our knowledge our work is the first to consider the special characteristics of the capacitor based system, illustrated in Fig. 3. We provide numerical results that demonstrate their effect.

Finally, we consider a *stochastic model* in which the energy inputs are i.i.d. random variable (e.g., a mobile device outdoor) and show how to treat it as a *Markov Decision Process*. We obtain policies (both for battery-based and capacitor-based systems) that can be pre-computed in advance. Namely, they can be provided as a tool to the device which would allow it

TABLE I
NOMENCLATURE

I	Irradiance (W/cm^2)
H	Irradiation (J/cm^2)
G	Energy harvested given device physical parameters (J)
Γ	Effective energy harvested (J)
K	Number of slots
B, B_1, B_{K+1}	Energy storage state, initial, and final levels (J)
C	Energy storage capacity
s	Energy spending rate (J/slot)
r	Data rate (bits/s)
c_{tx}	Energetic cost to transmit (J/bit)
c_{rx}	Energetic cost to receive (J/bit)
$U(\cdot)$	Utility function

to make decisions based on the current storage level and in some cases based on the current energy spending rate.

This paper is organized as follows. Section II describes related work and Section III presents the model. Section IV describes the measurements. Section V and VI describe algorithms for the predictable profile and stochastic models, respectively. Section VII briefly presents numerical results. We conclude and discuss future work in section VIII.

II. RELATED WORK

Predictable-profile: In [27], [29], duty cycle adaptations (mostly for *single nodes*) are considered. For a *network*, various metrics are considered including data collection rates [15], end-to-end packet delivery probability [48], data retrieval rate [49], and routing efficiency [33], [50]. Per-slot *short-term predictions* are assumed in [34].

Partially-predictable energy profile: while considering energy predictable, [29], [34], [37] have provisions for adjusting to where the predictions are not accurate.

Stochastic process: Dynamic activation of energy-harvesting sensors is described in [30]. Admission and power allocation control are developed in [16].

Model-free approach: Duty cycle adjustments for a *single node* (and under the *linear storage* model) are examined in [46]. A *capacitor*-based system is presented and the capacitor leakage is taken into account in [51].

Finally, additional related work includes examination of the variable duty cycle effect on network-wide parameters [22] and specific considerations for *indoor radiant energy harvesting* [21], [23], [41].

III. MODEL AND PRELIMINARIES

In this paper we focus both on light measurements and on resource allocation problems. The relationships between variables characterizing energy availability are shown in Fig. 4. Table I summarizes the notation.

Our measurements record *irradiance*, radiant energy incident onto surface (in W/cm^2), denoted by I . *Irradiation* H (in J/cm^2) is the integral of irradiance over a time period [12]. In our measurements I is sampled every Δt seconds, thus we calculate H_T as $H_T = \sum_T I(t)\Delta t$. In characterizing environments for light conditions, we are particularly interested in diurnal (daily) environmental energy availability. For

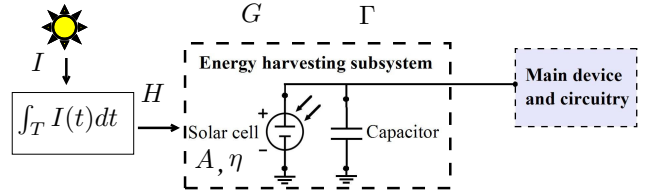


Fig. 4. A schematic diagram of the relationships between energy parameters: irradiance (I), irradiation (H), energy available to a device (G), and energy collected in storage (Γ).

$T = 24$ hours, we denote the *daily irradiation* by H_d . G (in J) is the amount of energy a device with the *given physical characteristics* has access to. For a device with solar cell size A and efficiency η , $G = A\eta H$.

We denote the energy storage capacity by C and the amount of energy stored by B ($0 \leq B \leq C$). When dealing with finite-horizon models, we denote the initial and the final energy levels by B_1 and B_{K+1} , respectively. We denote the energy spending rate by s .

The *effective* amount of energy a device can harvest from the environment is denoted by Γ . With *ideal (linear) storage*, $\Gamma = G$. However, Γ may depend not only on the available energy G , but also on the current energy level (see, for example, Fig. 3), that is, $\Gamma = q(G, B)$. We refer to storage models that exhibit the dependency on the current energy levels as *nonlinear storage models*.

We focus on *discrete-time* models, where the time axis is slotted, and a decision is made at the start of a slot. The ‘storage evolution’ for the models can be expressed as:

$$B(i+1) = \min\{B(i) + q(G(i), B(i)) - s(i), C\} \quad (1)$$

We consider the behavior of single (stand-alone) nodes and node pairs (links), denoted by u and v , whose data rates are $r_u(i)$ and $r_v(i)$. For single nodes we optimize the energy spending rate $s(i)$, which can be converted to *duty cycle*, *sensing rate*, or *communication rate*. For *links*, we assume that the energy spending rates of the are related, and thus optimize communication rates $r_u(i)$ and $r_v(i)$. We denote the costs to transmit and receive a bit by c_{tx} and c_{rx} .

Often the incoming energy varies throughout the day. We aim to achieve a *time-fair* resource allocation, that is, allocate, as much as possible, the energy in a uniform way with respect to time. We examine achieving this by using the *lexicographic maximization* and *utility maximization* frameworks. In the former, we lexicographically maximize the vector $\{s(1), \dots, s(K)\}$ (for a stand-alone node), or the vector $\{r_u(1), \dots, r_u(K), r_v(1), \dots, r_v(K)\}$ (for a link). Similar approaches have been applied to achieve fairness in data generation [15], [31] and in session rate allocations [13].

The network *utility maximization* framework is also well-developed [34], [38], but mostly for fairness amongst nodes, not across the different time slots.¹ To apply it, α -fair

¹Fair allocation of resources *along the time axis* is strongly tied to economics, most closely to economic *consumption smoothing* [18], which examines maintaining a stable spending level in the presence of income variations and uncertainties.

functions are used under a certain objective function that will be described in sections V and VI. α -fair functions are the family of *concave* and *non-decreasing* functions parameterized by $\alpha \geq 0$: $U_\alpha(\cdot) = (\cdot)^{1-\alpha}/1-\alpha$, for $\alpha \geq 0$, $\alpha \neq 1$ and $\log(\cdot)$ for $\alpha = 1$. Under our objective function, we use them to achieve max-min and proportional fairness [36]. We apply the utility maximization framework to find both the optimal spending rate $s(i)$ and the optimal communication rate $r(i)$.

IV. CHARACTERIZING LIGHT ENERGY

One of the important dimensions of the problem space is environmental energy modeling. Since large-scale *outdoor* solar panels have been used for many decades, properties of the Sun's energy were examined in depth [5], [32], [41]. In the sensor networking context, practical considerations regarding *outdoor* solar energy were discussed in [45]. Until recently using *indoor* radiant energy for networking applications was considered impractical, and therefore, indoor light was studied mostly in the architecture and ergonomics [17], [19], [24], [26], [43]. However, in these domains the important factor is *how humans perceive* a given light level (*photometric characterization* – i.e., measurements in Lux) rather than its *energy level* (*radiometric characterization* – i.e., measurements in W/cm^2) (*photometric* measurements by sensor nodes were also reported in [3], [23]). Since the human eye response to light differs from the solar cell's response, the photometric measurements do not provide energetic characterization and there is a lack of data (e.g., traces) and analysis (e.g., variability, predictability, and correlations) regarding energy availability [41].

To characterize indoor energy availability, since June 2009 we have been conducting a light measurement study in office buildings in New York City. In this study we take long-term measurements of *irradiance* (I , in units W/cm^2) in several indoor locations, and also study a set of shorter-term indoor/outdoor mobile device measurements. Table II provides a summary of the indoor measurement locations. Schematically, they are shown in Fig. 5. Note that the measurements in setups A-D and F are ongoing; the numerical analysis provided in the rest of this section corresponds to the data recorded by the installed setups up to fourth week of March, 2010. For the measurements we use TAOS TSL230rd photometric sensors [8] installed on LabJack U3 DAQ devices [4]. These photometric sensors have a high dynamic range, allowing capturing of widely varying irradiance conditions. We verified the accuracy of the sensors with a NIST-traceable [6] Newport 818-UV photodetector [7]. In addition to the indoor measurements, we also analyze a set of outdoor irradiance traces provided by the National Renewable Energy Laboratory (NREL) [5].

The provided measurements and *irradiance traces* can be used to determine the performance achievable by a particular device, for system design (e.g., choosing a suitable energy storage or energy harvesting system component), and for determining which algorithm to use. The traces we have collected can be also used as energy feeds to simulators and emulators.

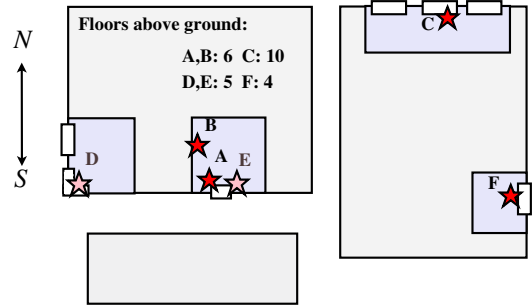


Fig. 5. A schematic diagram of the indoor irradiance measurement locations.

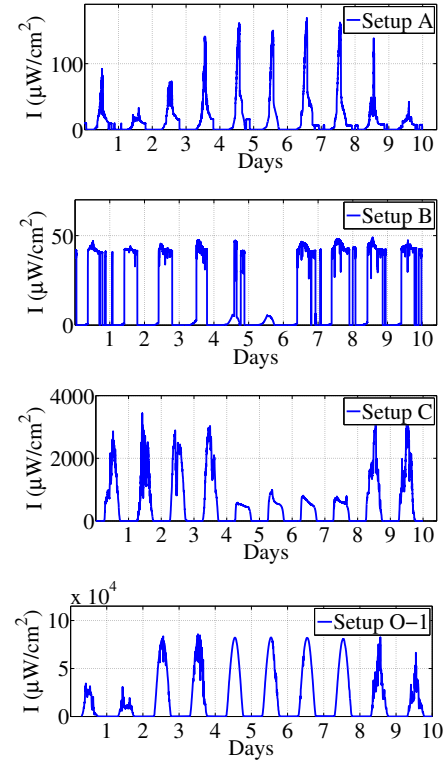


Fig. 6. Sample irradiance measurements in locations A, B, C, and O-1 (Mar. 2, 2010 - Mar. 12, 2010).

The traces will be made available in the CRAWDAD database [1].

A. Device Energy Budgets and Daily Energy Availability

Sample irradiance measurements (for setups A, B, C, and O-1 over the same 10 days) are provided in Fig. 6. One of the uses of the measurements is to determine *energy budgets* for indoor energy-harvesting devices. Using the recorded irradiance, we calculate the total daily *irradiation* H_d , representing energy incident onto $1cm^2$ area over the entire course of a day. Fig. 7 demonstrates the H_d values for setup A recorded for over 300 days, and for setup E recorder over more than 100 days. Table II presents the mean and the standard deviation values \bar{H}_d and $\sigma(H_d)$. This table also includes the data rates a node would be able to maintain throughout a day when exposed to irradiation H_d . These data rates are calculated

TABLE II
RADIANT ENERGY MEASUREMENT SETUPS, AVERAGE DAILY IRRADIATION, AND ACHIEVABLE DATA RATES.

Location index	Location description	Experiment timeline	$\overline{H_d}$ (J/cm ² /day)	$\sigma(H_d)$	r (Kb/s, cont.)
A	Students' office, South-facing, 6th floor above ground; measurement setup located on a windowsill; shading is used at all times.	Aug. 2009 –	1.43	0.8	1.6
B	Students' office (same as setup A); setup on a bookshelf far from the window, receiving direct sunlight for a short portion of a day.	Nov. 2009 –	1.29	0.78	1.5
C	Departmental conference room, North-facing, with large windows and an unobstructed view; setup located on a windowsill. Shading use varies (corresponding to the needs and preferences of different affiliates using the conference room).	Nov. 2009 –	26.6	13.7	30.1
D	Students' office; corner window facing South and West; setup placed on a windowsill, shading extensively used	Nov. 2009 –	3.46	1.69	4.0
E	Students' office directly under the office of setup A; setup on a windowsill, limited use of shading.	Jun. 2009 – Oct. 2009	12.3	8.3	13.9
F	Students' office, East-facing; setup on a windowsill; office window often kept partially opened (the setup often receives unattenuated reflected outdoor light).	Feb. 2010 –	97.3	64.4	112.3
O-1	Outdoor: ECSU meteorstation [5], Elizabeth City, NC.	Jan. 2009 –	1152	510	1,300
O-2	Outdoor: Humboldt State University meteorstation [5], Arcata, CA.	Jan. 2009 –	1805	740	2,100

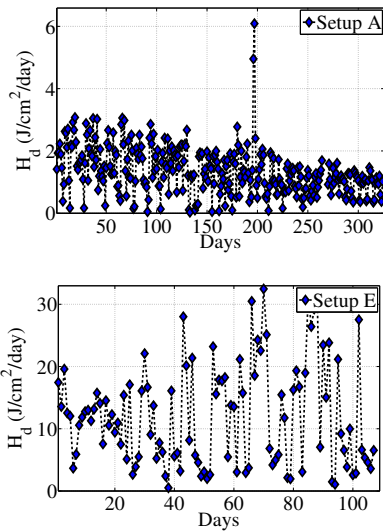


Fig. 7. Long-term daily irradiation (H_d) for setups A (Aug. 15, 2009 – July 6, 2010) and E (June 25, 2009 – Nov. 11, 2009)

assuming the *solar cell efficiency* $\eta = 1\%$ (i.e., efficiency of an organic solar cell [21]) and *solar cell size* $A = 10\text{cm}^2$ (i.e., square solar panel with side length 3.16 cm). As an energy cost to communicate, 1nJ/bit is used [21] – that is, the bit rate r is calculated as $r = [A \cdot \eta \cdot H_d / (3600 \cdot 24)] / (1 \cdot 10^{-9})$.

We note that for the different indoor setups the H_d values vary greatly, from under 2 J/cm^2 (i.e., setups A and B), to over 97 J/cm^2 (setup F). These differences are related to presence or absence of direct sunlight, the use of shading, windows, and indoor lights, as well as office layouts. Setup A, for example, is located in an office where shading is extensively used. Setup F, on the other hand, is located near a window kept partially opened, receiving outdoor light not attenuated by window glass, and thus receiving much more energy than other setups.

To predict *daily energy availability* H_d , a node can use a simple *exponential smoothing* approach, calculating a predictor for slot i , $\widehat{H}_d(i)$, as $\widehat{H}_d(1) \leftarrow H_d(0)$, $\widehat{H}_d(i) \leftarrow \alpha \cdot H_d(i-1) + (1-\alpha) \cdot \widehat{H}_d(i-1)$ for α constant, $0 \leq \alpha \leq 1$ [25]. The error for such simple predictors is relatively high. For example, for setup A the average prediction error is over

$0.4\overline{H_d}$, and for setup F the average prediction error is over $0.5\overline{H_d}$. For the outdoor datasets the average prediction errors are approximately $0.3\overline{H_d}$.

Improving the energy predictions (for outdoor conditions) using *weather forecasts* has been studied in [32], [44]. We studied whether the H_d values in the *indoor settings* were correlated with the weather. We used the weather conditions provided by [10] as the simple weather forecast. In [10], six categories for weather conditions are used ('sunny', 'partly sunny', 'partly cloudy', 'overcast', 'snow', and 'rain'). We grouped 'rain' and 'snow' in one category ('precipitation'), and assigned numerical integer values from 1 ('precipitation') to 5 ('sunny') as a weather state for each corresponding day. This simple scheme was used to represent commonly available daily energy forecasts. We determined substantial correlations with the weather conditions for some of the *indoor* locations. For example, for setup A the correlation coefficient of H_d values with the weather data is $r_c = 0.46$ ($p < .001$), and for setup F it is $r_c = 0.8$ ($p < .001$). This suggests that for some indoor setups the energy predictions may be improved, similar to outdoor environments, by incorporating the weather forecasts into the predictions.

Work week pattern also influences indoor radiant energy in office environments, particularly for setups that do not receive direct sunlight. For setup B, for example, $\overline{H_d} = 1.61\text{ J/cm}^2$ on weekdays, and $\overline{H_d} = 0.46\text{ J/cm}^2$ on weekends (it receives, on average, 9.7h of office lighting per day on weekdays and under 1h on weekends). By keeping separate predictors for weekends and weekdays, the average prediction error for the weekdays is lowered from $0.47\overline{H_d}$ to $0.28\overline{H_d}$. Similarly, for setup A, where $\overline{H_d} = 1.56\text{ J/cm}^2$ on weekdays and $\overline{H_d} = 1.13\text{ J/cm}^2$ on weekends, keeping separate predictors for weekends and weekdays lowers the average error for the weekdays from $0.4\overline{H_d}$ to $0.34\overline{H_d}$.

We also studied correlations between H_d values of different datasets, and determined statistically significant correlations for a number of setups. For example, for setups A and B located in the same room, $r_c = 0.48$ ($p < .001$), and for setups A and E facing in the same direction, $r_c = 0.71$ ($p < .001$). This indicates that in a *network* where devices are *subject to the common stimuli through their energy harvesting channels*,

a device will be able to infer its peers' energy availability based on its own (locally observed) energy state.

B. Short Term Energy Profiles

To characterize energy availability at different times of day, we determine the H_T values for different 0.5 hour intervals T , thus generating *energy profiles* for the setups. Sample energy profiles are shown in Fig. 8, where the left hand side shows the irradiance curves from different days for a setup overlaid with each other, and the right hand side shows the $\overline{H_T}$ values, with errorbars representing $\sigma(H_T)$. Due to indoor location setup, illumination, and occupancy patterns, the energy profiles of different indoor locations can be very different. For example, while Setup C shows daylight-dependent variations in irradiance level, setup B receives the irradiance of either 0 or $45 \mu\text{W}/\text{cm}^2$ for most of the day (as it is mostly illuminated by indoor lights). In addition, while in setup B the lights are often on during evening hours, in setup C it is almost never the case. The demonstrated $\sigma(H_T)$ values suggest that these energy inputs generally fall under the *partially predictable profile* energy models.

We have studied whether, similarly to outdoor scenarios [11], [32], in the indoor datasets the profile characterization *for a given day* can be improved when a device has observed some of the daily energy. We looked at the correlations between the amount of energy H_T in a given slot and the amount of energy in the subsequent slots, as well as at the correlations between the amount of energy collected up to a particular time of day and the energy in the rest of the day.

We have observed that generally these correlations are stronger for outdoor datasets than for indoor datasets. For example, for outdoor setup O-1, the correlation between the amount of energy received before 8 am and the amount of energy it received after 8 am is $r_c = 0.77$ ($p < .001$), while for setup C it is $r_c = 0.31$ ($p < .001$). As another example, for setup O-1, the correlation between the energy it gets at 10:30 am and the energy it gets at 16:30 am is $r_c = 0.5$, while for setup A it is $r_c = 0.2$. This indicates that overall the outside energy is more predictable; however, it also indicates that profile prediction techniques developed for adjusting energy profile predictions in the outside systems may be extended to the indoor systems.

C. Mobile Measurements

We have also conducted shorter-term experiments for mobile devices. Table III provides a summary of the measurements conducted. Fig. 9 demonstrates a set of irradiance traces in different conditions. We observed that mobile devices' energy levels are poorly predictable and could in some cases be represented by *stochastic* energy models.

Measurements M-1, shown in Fig. 9(a), highlight the disparity between the light energy available indoors and outdoors. In this trace, as the device is moved from the indoor lab to the outside, the irradiance changes from $70 \mu\text{W}/\text{cm}^2$ to 32mW – that is, the ratio is more than 450 times. Measurements M-6, shown in Fig. 9(c), demonstrate the irradiance recorded by a

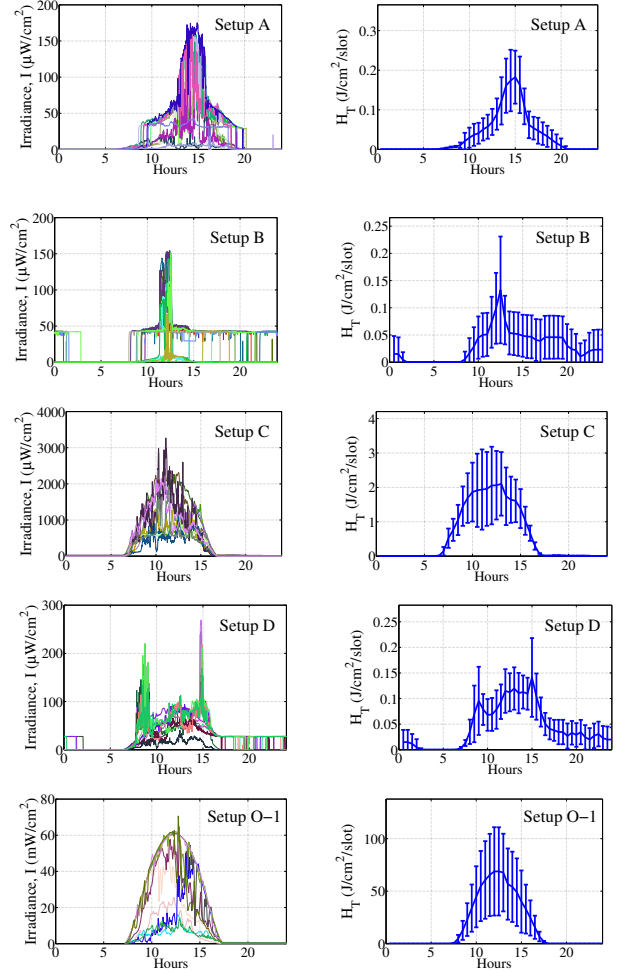


Fig. 8. Sample *energy profiles* for indoor locations A, B, C, and D, and for the outdoor installation O-1. Left: irradiance measurements from different days, overlaid; Right: $\overline{H_T}$ values, with errorbars representing $\sigma(H_T)$.

TABLE III
MOBILE MEASUREMENTS SUMMARY

Meas. index	Meas. description	Date	Time
M-1	Pedestrian walking around university campus (indoor and outdoor environments) carrying a sensor.	4/5/2010	13:06-14:10
M-2	Commuting on public transit, sensor attached to a backpack, measurements outdoors, indoors (subway, train, office).	7/13/2010	15:02-16:42
M-3	Car-based roadtrip (sensor attached to the dashboard).	7/16/2010	12:26-15:23
M-4	Car-based errand running, afternoon, sensor attached to the dashboard.	7/17/2010	14:48-17:04
M-5	Car-based errand running, sensor attached to the dashboard, morning.	7/18/2010	09:58-12:05
M-6	Pedestrian walking in New York City at nighttime (Theater District and Times Square), sensor attached to a backpack.	7/22/2010	20:02-21:36

mobile device in New York City's Theater District and Times Square at nighttime. We observed that the energy available at nighttime in these locations is comparable to the energy of brightly lit indoor office environments.

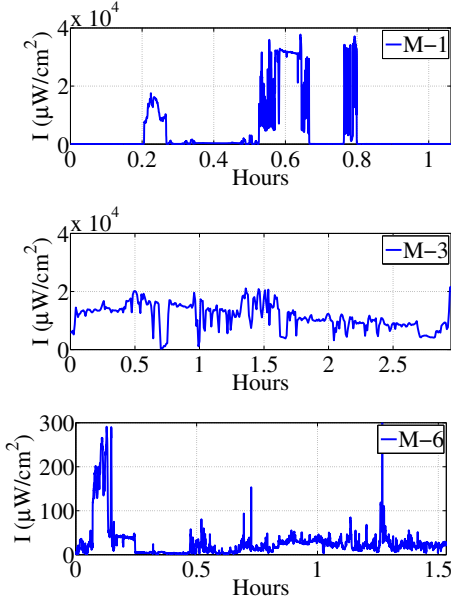


Fig. 9. Sample irradiance measurements recorded by mobile devices.

V. PREDICTABLE ENERGY PROFILE MODEL

In this section we consider the *predictable profile* energy model (similar to the models studied in [15], [29], [37]). We formulate optimization problems that apply to both *linear* and *nonlinear* energy storage for a single node and for pair-wise nodes (link). We show that for linear storage, the problems can be solved by simple algorithms.

A. Single Node: Optimizing Energy Spending

To smooth the node's energy spending, we formulate the following problems using *lexicographic maximization* and *utility maximization* frameworks.

Time Fair Lexicographic Assignment (TFLA) Problem:

$$\text{Lexicographically maximize: } \{s(1), s(2), \dots, s(K)\} \quad (2)$$

$$\text{s.t.:} \quad s(i) \leq B(i) \quad \forall i \quad (3)$$

$$B(i) \leq B(i-1) + \Gamma(i-1) - s(i-1) \quad \forall i \geq 2 \quad (4)$$

$$B(i) \leq C \quad \forall i \quad (5)$$

$$B(1) = B_1; \quad B(K) + \Gamma(K) - s(K) \geq B_{K+1} \quad (6)$$

$$B(i), s(i) \geq 0 \quad \forall i \quad (7)$$

Recall that $\Gamma(i) = q(G(i), B(i))$. Constraint (3) ensures that a node does not spend more energy than it has stored, (4) and (5) represent the storage evolution dynamics, and (6) sets starting storage level to B_1 and ensures that the final storage level is at least B_{K+1} .

Time Fair Utility Maximization (TFU) Problem:

$$\max_{s(i)} \sum_{i=1}^K U(s(i)) \quad (8)$$

$$\text{s.t.: constraints (3) – (7)}$$

The constraints set is convex for both linear and non-linear storage models. For linear storage ($\Gamma = G$), we refer to the above problems as *TFLA-LIN* and *TFU-LIN*, respectively.

Observation 1: The optimal *TFLA-LIN* and the optimal *TFU-LIN* solutions are equal.

Proof: Given in Appendix I. ■

The problem *TFLA-LIN* can be solved by iteratively solving a set of linear programming problems as follows:

Procedure Linsolve: Define A_{fix} to be the set of slot indexes for which the lexicographically maximal spending level $s(i)$ has been determined. Starting with $A_{fix} = \emptyset$, iteratively solve the following linear programming sub-problem:

$$\tilde{s} = \max \min s(i) \text{ over all } i \notin A_{fix} \quad (9)$$

$$\text{s. t.: constraints (3) – (7)}$$

Solving an instance of problem (21) identifies the max min spending level $s(i) = \tilde{s}$ for one or more slots i ; the corresponding slot indexes i are moved to the set A_{fix} . At the first iteration, $A_{fix} = \emptyset$, and problem (21) considers the entire K slots. With each iteration, at least one spending level value $s(i)$ is determined, and the corresponding index i is moved into the A_{fix} set. Thus, obtaining the optimal solution for the *TFLA-LIN* problem requires solving at most K linear programming problems, and the LP size is reduced with every step of the procedure.

Below we provide an algorithm, inspired by algorithms for max–min fair flow control [13], that can be used to find the optimal spending rate $s(i)$ *without solving linear programming problems*, and thus can be implemented by devices with limited computational capabilities. **Progressive Filling Algorithm (PFA)** (Alg. 1): the algorithm starts with $s(i) \leftarrow 0 \quad \forall i$, and iterates through slots 1 to K , increasing the spendings of each slot by ϵ . When an increase in $s(i)$ for a slot i is considered, the algorithm verifies that the increase would not result in shortage of energy for other slots, or lack of final energy B_{K+1} . When this verification fails, the spending level of slot i gets ‘fixed’ at $s(i)$, and the progressive filling continues for the slots that are not yet fixed. In each step of the algorithm, we either increase $s(i)$ or fix slot i . The spending level of a slot is increased only when it does not interfere with the spending of slots with lesser spending levels, thus the resulting solution is max-min fair.

Finally, in the special **Large Linear Storage (LLS)** where the *energy storage is large compared to the harvesting rate* both *TFLA-LIN* and *TFU-LIN* can be solved easily. For *LLS*, the optimal solution for both problems is to spend in each slot i the average of the total energy available, $s^* = \lceil \sum_{i=1}^K G(i) + (B_1 - B_{K+1}) \rceil / K$. Below, we first show the conditions under which this solution is feasible. Then we show that, where feasible, it is optimal.

To specify the *LLS* conditions, we define $\tilde{B}(i) = \lceil \sum_{n=1}^{i-1} G(n) \rceil - s^* \cdot (i-1)$ for $2 \leq i \leq K+1$. Then the following lemma holds:

Lemma 1: When $B_1 \geq \lceil \min_{2 \leq i \leq K} \tilde{B}(i) \rceil$ and $C - B_1 \geq \max_{2 \leq i \leq K} \tilde{B}(i)$, the s^* -policy is feasible.

Algorithm 1 Progressive Filling Algorithm (PFA):

```

 $A_{fix} \leftarrow \emptyset; s(i) \leftarrow 0 \forall i;$ 
while  $A_{fix} \neq \emptyset$ 
  for  $i = 1; i \leq K; i ++;$  do
    if  $i \in A_{fix}$  then
       $\tilde{s} \leftarrow s; \tilde{s}(i) \leftarrow \tilde{s}(i) + \epsilon;$ 
       $valid \leftarrow \text{check\_validity}(\tilde{s});$ 
      if  $valid == TRUE$  then  $s(i) \leftarrow \tilde{s}(i);$ 
      else  $A_{fix} := A_{fix} \cup i;$ 
    function  $\text{check\_validity}(\tilde{s}):$ 
       $B(i) \leftarrow 0 \forall i; B(1) \leftarrow B_1; valid \leftarrow TRUE;$ 
      for  $i = 2; i \leq K; i ++;$  do
         $B(i) \leftarrow \min(C, B(i-1) + q(G(i-1), B(i-1)) - \tilde{s}(i-1))$ 
        if  $\tilde{s}(i) > B(i)$  then  $valid \leftarrow FALSE;$ 
         $\tilde{B}_f \leftarrow B(K) + q(G(K), B(K)) - \tilde{s}(K);$ 
        if  $B_{K+1} < \tilde{B}_f$  then  $valid \leftarrow FALSE$ 
      return  $valid$ 

```

Proof: Assume the energy storage capacity is sufficiently large. Then the storage state under the s^* -policy at the beginning of the i^{th} slot is $B(i) = B_1 + [\sum_{n=1}^{i-1} G(n)] - s^* \cdot (i-1) = B_1 + \tilde{B}(i)$. Thus, to avoid running out of energy, $B_1 \geq \lfloor \min_{2 \leq i \leq K} \tilde{B}(i) \rfloor$ is needed. In addition, in each slot i , $C - B(i) \geq 0$ is required. Plugging in the expression for $B(i)$, the condition $C - B_1 \geq \max_{2 \leq i \leq K} \tilde{B}(i)$ is obtained. ■

It is straightforward to show that for *TFLA-LIN* the s^* -policy is optimal (when feasible). Constraints (4) and (6) imply that any other vector s in the feasible domain has at least one i such that $s(i) \leq s^*$. Hence the s^* -policy is the optimal solution to *TFLA-LIN*.

Proposition 1: The s^* -policy (if feasible) is the optimal solution for the *TFU-LIN* problem.

Proof: Given in Appendix II. ■

Note that both the *LLS* conditions and the simple *LLS* solution can be easily calculated.

B. Link: Optimizing Data Rates

For a *link*, we extend the optimization problems, for the lexicographic and utility maximization frameworks, as follows.

Pairwise Time Fair Lexicographic Assignment (P-TFLA) Problem:

Lexicographically maximize:

$$\{r_u(1), r_u(2), \dots, r_u(K), r_v(1), r_v(2), \dots, r_v(K)\} \quad (10)$$

$$\text{s.t. :} \quad c_{\text{rx}} r_u(i) + c_{\text{rx}} r_v(i) \leq s_u(i) \quad (11)$$

$$c_{\text{rx}} r_v(i) + c_{\text{rx}} r_u(i) \leq s_v(i) \quad (12)$$

$$u, v : \text{constraints (3) - (7)}$$

Pairwise Time Fair Utility Maximization (P-TFU) Problem:

$$\max_{r_u(i), r_v(i)} \sum_{i=1}^K [U(r_u(i)) + U(r_v(i))] \quad (13)$$

$$\text{s.t.:} \quad (11), (12)$$

$$u, v : \text{constraints (3) - (7)}$$

For linear energy storage, formulation *P-TLFA* can be solved by a straightforward extension of the *PFA*, provided for completeness in Appendix III.

Note that unlike in the single-node case examined in the previous section, the two frameworks do not result in the same solution. When solving *P-TFLA*, for the given i , $r_u(i) = r_v(i)$. Under the lexicographic formulation, in a slot we maximize the minimum rate, the best solution is the same rate for both. The utility maximization framework of problem *P-TFUA*, on the other hand, adjusts transmit/receive to use all energy possible, having one rate go lower and another one go higher.

For small devices with limited computational capabilities solving the *P-TFUA* problem directly may be computationally taxing. Instead, the nodes may use the following heuristic algorithm, which is easy to solve and does not require extensive exchange of information:

Separate Rate Determination (SRD) Algorithm: The algorithm starts with nodes u and v determining *independently from each other* their energy spending rates $s_u(i)$ and $s_v(i)$ for every slot i (i.e., using the *PFA* algorithm). Then, they solve:

$$\begin{aligned} \max_{r_u(i), r_v(i)} \quad & U(r_u(i)) + U(r_v(i)) \quad (14) \\ \text{s.t.:} \quad & \text{constraints (11), (12)} \end{aligned}$$

Problem (14) can be easily solved. For example, Appendix IV details the algebraic solution to this problem for the objective function $U(r) = \log(r)$. In section VII we will provide numerical results that demonstrate the rates $\{r_u(i), r_v(i)\}$ obtained by using the SRD and by using the *P-TFLA* and *P-TFU*.

VI. STOCHASTIC ENERGY MODELS

In this section we study models in which the energy harvested in a slot is an *i.i.d. random variable* G . G may represent, for example, the energy harvested by a *mobile* device in a short (seconds or minutes) time slot. For time slots of *days*, it may represent the *daily irradiation* H_d received by a device.² We formulate the spending rate control problems and determine corresponding policies for a single node, including additional considerations for the *cost of changing the rate*. We also show a formulation taking into account the dependency between two nodes. The formulations apply to *linear* and *nonlinear* energy storage models. For a given G , the optimal policy needs to be calculated *once*, thus operating according to the optimal policy does not require frequent computations.

For tractability, we use *quantized* energy storage state B and harvested energy G values: $B \in \{0, \dots, C\}$, and G takes discrete values $[g_1, \dots, g_M]$ with probability $[p_1, \dots, p_M]$.

Spending Policy Determination (SPD) Problem: For a given G , *determine the energy spending rate* $s(B(i))$ for each state

²When the energy storage is relatively large, variations in energy availability *within* a day may be abstracted, and H_d can be used to characterize energy availability.

$B(i)$ such that:

$$\max_{s(B(i))} \lim_{K \rightarrow \infty} \frac{1}{K} \sum_{i=1}^K U(s(B(i))). \quad (15)$$

This *discrete time stochastic control process* is a *Markov Decision Process* (MDP) which can be solved in a number of ways. In Appendix V we show how the *Policy Improvement Algorithm* can be applied to this problem; below, we focus on *dynamic programming* approaches. The state of the system at time i is fully described by $\{B(i)\}$. Applying dynamic programming, we consider a large number of slots, and going ‘backwards’ from the last slot, for each storage state $B(i)$ maximize the following:

$$\begin{aligned} h(i, B(i)) &= \max_{s(i) \leq B(i)} \mathbb{E}_G[U(s(i)) + \\ &h(i+1, \min[B(i) + \Gamma(i) - s(i), C])] = \\ &\max_{s(i) \leq B(i)} [U(s(i)) + \sum_{g \in G} p_g \\ &\cdot h(i+1, \min[B(i) + q(g, B(i)) - s(i), C])]. \end{aligned} \quad (16)$$

Solving this iterative procedure for a large number of slots results in a policy $s(B(i))$ that approaches the optimal policy $s(B)$.

The MDP formulation can be easily extended to take additional parameters into account. Below, we extend it for the case where *changing the spending rate has a cost* (i.e., nodes have to coordinate the change). For such case the state of the system at time i is described by a tuple $\{B(i), s_p(i)\}$ where s_p denotes the spending rate in use prior to time i .

Spending Policy Determination with Cost to Change (SPD-CC) Problem:

$$\max_{s(B(i), s_p(i))} \lim_{K \rightarrow \infty} \frac{1}{K} \sum_{i=1}^K U[s(B(i), s_p(i)), s_p(i)] \quad (17)$$

where the utility function depends on both $s(i)$ and $s_p(i)$. For example, for a cost to change defined as c_1 times the change magnitude, $U(s(i), s_p(i)) = U(s(i)) - c_1 |s(i) - s_p(i)|$. The following dynamic programming formulation can be used to solve this problem:

$$\begin{aligned} h(i, B(i), s_p(i)) &= \max_{s(i): s(i) \leq B(i)} [U(s(i), s_p(i)) + \\ &\sum_{g \in G} p_g \cdot h(i+1, \min[B(i) + q(g, B(i)) - s(i), C])] \end{aligned} \quad (18)$$

We note that this relates to existing work in the area of *stochastic dam processes*. For example, [14] examines a case of water flowing into a finite reservoir according to a Wiener process, and being released continuously, where a cost is associated with the change of release rate.

The Markov Decision Process formulation can also be extended to a *link* as follows:

Link Spending Policy Determination (L-SPD):

$$\max_{s_u(i), s_v(i)} \lim_{K \rightarrow \infty} \frac{1}{K} \sum_{i=1}^K U(\{s_u(i), s_v(i)\}) \quad (19)$$

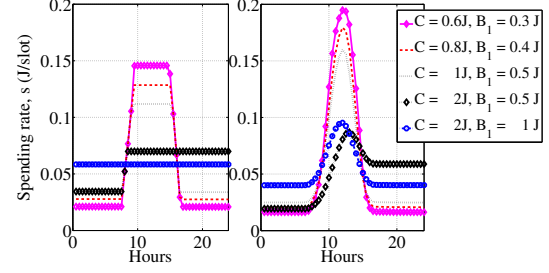


Fig. 11. Energy spending rates $s(i)$: obtained by solving *TFLA* problem for *linear energy storage* (left), and by solving the *TFU* problem for *nonlinear energy storage* (right).

where $\{s_u(i), s_v(i)\}$ are a function of $\{(B_u, B_v)\}$. The dynamic programming formulation for it is as follows:

$$\begin{aligned} h(i, [B_u(i), B_v(i)]) &= \\ &\max_{s_u(i): s_u(i) \leq B_u(i); s_v(i): s_v(i) \leq B_v(i)} \mathbb{E}_{G_u, G_v} [U(s_u(i), s_v(i)) \\ &+ h(i+1, [\min[B_u(i) + \Gamma_u(g_u, B_u(i)) - s_u(i), C_u], \\ &[\min[B_v(i) + \Gamma_v(g_v, B_v(i)) - s_v(i), C_v]])] \end{aligned} \quad (20)$$

Computationally, problems *SPD-CC* and *L-SPD* can be approached similarly to problem *SPD*. Despite that due to their extended state space they are computationally expensive to solve, recall that the policies need to be computed only once. In the next section the sample optimal policies obtained by solving problems *SPD* and *SPD-CC* are provided.

VII. NUMERICAL RESULTS

This section provides numerical results that demonstrate the use of the algorithms described in Sections V and VI. Measurements described in Section IV are used as inputs to the algorithms. Fig. 11 shows the solutions for the *TFLA* and the *TFU* optimal energy spending rate determination problems of Section V-A. The energy profile of setup *C* (see Fig. 8) is used as an input to the algorithms. The left side of Fig. 11 shows the spending rates $s(i)$ that solve the *TFLA-LIN* problem. These spending rates are obtained using the *PFA* algorithm. The right side of Fig. 11 shows the solutions of the *TFU* problem for the *energy storage with storage state-dependent inputs*, which has not been analyzed before.

Fig. 10 shows the numerical results for the link rate determination problems described in Section V-B. The energy profiles of setups *A* and *B* (see Fig. 8) are used as inputs for the algorithms. The left side of Fig. 10 shows the optimal communication rates $\{r_u(i), r_v(i)\}$ obtained by solving the *P-TFLA* and *P-TFU* problems for linear storage. While the lexicographically defined problem *P-TFLA* is optimized when $r_u(i) = r_v(i)$ for each i , the utility maximization-based *P-TFU* problem determines different rates $r_u(i)$ and $r_v(i)$. The middle graph in Fig. 10 demonstrates the rates $r_u(i)$ and $r_v(i)$ calculated using the simple heuristic algorithm *SRD*. It can be seen that the *SRD* algorithm obtains communication rates $r_u(i)$ and $r_v(i)$ that are similar to those obtained by solving the *P-TFU* problem. Finally, the rightmost graph in Fig. 10

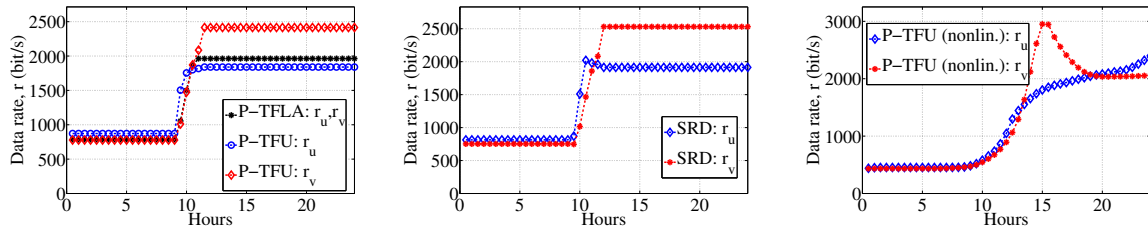


Fig. 10. Communication rates $r_u(i)$ and $r_v(i)$: obtained by solving the P -TFLA and P -TFU problems for *linear energy storage* (left), calculated with the heuristic algorithm SRD (middle), and obtained by solving the P -TFU problem for *nonlinear storage* (right).

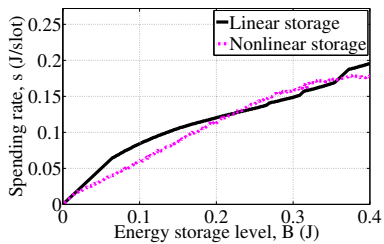


Fig. 12. Optimal policies $s(B)$ obtained by solving the SPD problem, shown for *linear* and *nonlinear* energy storage.

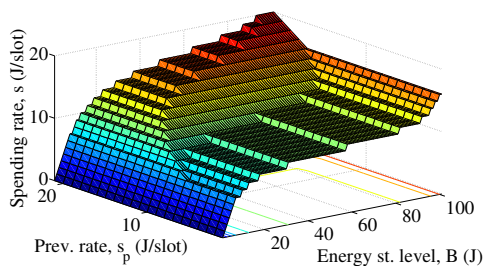


Fig. 13. Optimal policy $s(B, s_p)$ obtained by solving the SPD -CC problem.

presents an example of the solution to the P -TFU problem for *nonlinear energy storage*.

Fig. 12 and 13 illustrate the *optimal energy spending policies* obtained by solving the SPD (Fig. 12) and the SPD -CC (Fig. 13) problems defined in Section VI. The daily irradiation H_d for setup A is used as the random variable G . Fig. 12 shows the optimal policies $s(B)$ for *linear* and *nonlinear* energy storage types. We note that again the optimal policies are different. Fig. 13 shows the optimal energy spending rate determination policy $s(B(i), s_p(i))$, where, as there is cost associated with changing the spending rate, the spending rate $s(i)$ is a function of both the level of energy storage B and the past spending rate $s_p(i)$.

VIII. CONCLUSIONS AND FUTURE WORK

Motivated by recent advances in the areas of energy harvesting and ultra-low-power communications, in this paper we focused on energy harvesting networks. We described a long-term indoor radiant energy measurements campaign that provides useful traces, as well as insights into the design of systems and algorithms. We developed simple algorithms for predictable environment that uniquely consider the spending

policies for energy storage with storage state-dependent inputs. The algorithms for the predictable case also provide insight into the partially-predictable case. We developed algorithms for stochastic environments that can provide nodes with simple pre-computed decisions policies. We used the algorithms to obtain numerical results for various cases.

This paper covered a few “working points” in the design space described in Section I. Yet, there are still many other working points to study. In particular, although some algorithms have been developed for networks of nodes, most of them are too complex for resource-constrained nodes. Hence, we plan to develop simple energy-harvesting-aware algorithms for networks of nodes considering the various other problem dimensions. Moreover, we plan to evaluate these algorithm in an EnHANTs testbed that we are currently building [20].

IX. ACKNOWLEDGEMENTS

This work was supported in part by the Vodafone Americas Foundation Wireless Innovation Project, Google Inc., NSF grants CNS-0916263 and CCF-0964497, and by an NSERC CGS grant. We thank Matthias Bahlke, Enlin Xu and Michael Zapas for their assistance with the indoor radiant energy measurements. We also thank Peter Kinget and John Kymissis for helpful discussions.

REFERENCES

- [1] “CRAWDAD – a community resource for archiving wireless data,” crawdad.cs.dartmouth.edu/.
- [2] “Cymbet EnerChips;,” www.cymbet.com/content/products.asp.
- [3] “Intel Lab data,” db.csail.mit.edu/labdata/labdata.html.
- [4] “LabJack U3 USB-based multifunction data acquisition and control device,” labjack.com/.
- [5] “Measurement and Instrumentation Data Center, National Renewable Energy Laboratory (NREL), US Dept. of Energy;,” www.nrel.gov/mid/.
- [6] “National Institute of Standards and Technology (NIST);,” www.nist.gov/.
- [7] “Newport 818-UV low-power photodetector;,” www.newport.com/.
- [8] “TAOS TSL230rd programmable light-to-frequency converter;,” www.taosinc.com/.
- [9] “Texas Instruments MSP430 Solar Energy Harvesting Development Tool;,” focus.ti.com/docs/toolsw/folders/print/ez430-rf2500-seh.html.
- [10] “Weather Underground Weather History and Data Archive;,” www.wunderground.com/history/.
- [11] M. I. Ali, B. M. Al-Hashimi, J. Recas, and D. Atienza, “Evaluation and design exploration of solar harvested-energy prediction algorithm,” in *Design, Automation and Test in Europe (DATE’10)*, Mar. 2010.
- [12] W. Benenson, J. Harris, H. Stocker, and H. Lutz, *Handbook of Physics*. Springer, 2002.
- [13] D. Bertsekas and R. Gallager, *Data Networks*, 2nd ed. Prentice-Hall, 1992.

- [14] M. J. Faddy, "Optimal control of finite dams: Continuous output procedure," *Advances in Applied Probability*, vol. 6(4), pp. 689–710, 1974.
- [15] K.-W. Fan, Z. Zheng, and P. Sinha, "Steady and fair rate allocation for rechargeable sensors in perpetual sensor networks," in *Proc. ACM SenSys'08*, Nov. 2008.
- [16] M. Gatzianas, L. Georgiadis, and L. Tassioulas, "Control of wireless networks with rechargeable batteries," *IEEE Trans. Wireless. Comm.*, vol. 9, no. 2, pp. 581–593, 2010.
- [17] R. Gifford, "Light, Decor, Arousal, Comfort and Communication," *J. Environm. Psychology*, vol. 8, no. 3, pp. 177–189, 1988.
- [18] C. Gollier, *The Economics of Risk and Time*. McGraw-Hill, 2001.
- [19] G. Gordon, *Interior Lighting for Designers*, 4th ed. Wiley, 2003.
- [20] M. Gorlatova, T. Sharma, D. Shrestha, E. Xu, J. Chen, A. Skolnik, D. Piao, P. Kinget, I. Kymissis, D. Rubenstein, and G. Zussman, "Demo: Prototyping Energy Harvesting Active Networked Tags (EnHANTs) with MICA2 motes," in *Proc. IEEE SECON'10*, June 2010.
- [21] M. Gorlatova, P. Kinget, I. Kymissis, D. Rubenstein, X. Wang, and G. Zussman, "Challenge: ultra-low-power energy-harvesting active networked tags (EnHANTs)," in *Proc. ACM MobiCom'09*, Sept. 2009.
- [22] Y. Gu, T. Zhu, and T. He, "ESC: Energy synchronized communication in sustainable sensor networks," in *Proc. IEEE ICNP'09*, Oct. 2009.
- [23] J. Gummesson, S. S. Clark, K. Fu, and D. Ganesan, "On the limits of effective micro-energy harvesting on mobile CRFID sensors," in *Proc. ACM MobiSys'10*, June 2010.
- [24] D. Heil and S. Mathis, "Characterizing free-living light exposure using a wrist-worn light monitor," *Applied Ergonomics*, vol. 33, no. 4, pp. 357–363, 2002.
- [25] F. S. Hillier and G. J. Lieberman, *Introduction to Operations Research*, 6th ed. McGraw-Hill, 1995.
- [26] R. Hopkinson, *Architectural Physics: Lighting*. H.M.S.O., 1963.
- [27] J. Hsu, S. Zahedi, A. Kansal, M. Srivastava, and V. Raghunathan, "Adaptive duty cycling for energy harvesting systems," in *Proc. IEEE ISLPED'06*, Oct. 2006.
- [28] X. Jiang, J. Polastre, and D. Culler, "Perpetual environmentally powered sensor networks," in *Proc. IEEE IPSN'05*, Apr. 2005.
- [29] A. Kansal, J. Hsu, S. Zahedi, and M. B. Srivastava, "Power management in energy harvesting sensor networks," *ACM Trans. Embedded Comput. Syst.*, vol. 6, no. 4, 2007.
- [30] K. Kar, A. Krishnamurthy, and N. Jaggi, "Dynamic node activation in networks of rechargeable sensors," *IEEE/ACM Trans. Netw.*, vol. 14, no. 1, pp. 15–26, 2006.
- [31] F. P. Kelly, A. Maulloo, and D. Tan, "Rate control in communication networks: shadow prices, proportional fairness and stability," *J. Oper. Res. Soc.*, vol. 49, pp. 237–252, 1998.
- [32] M. Kudo, A. Takeuchi, Y. Nozaki, H. Endo, and J. Sumita, "Forecasting electric power generation in a photovoltaic power system for an energy network," *Electrical Eng. in Japan*, vol. 167, no. 4, pp. 16–23, 2009.
- [33] L. Lin, N. Shroff, and R. Srikant, "Asymptotically optimal energy-aware routing for multihop wireless networks with renewable energy sources," *IEEE/ACM Trans. Netw.*, vol. 15, no. 5, pp. 1021–1034, 2007.
- [34] R.-S. Liu, P. Sinha, and C. E. Koksal, "Joint energy management and resource allocation in rechargeable sensor networks," in *Proc. IEEE INFOCOM'10*, Mar. 2010.
- [35] X. Lu and S. Yang, "Solar energy harvesting for ZigBee electronics," *Sustainability in Energy and Buildings*, pp. 19–27, 2009.
- [36] J. Mo and J. Walrand, "Fair end-to-end window-based congestion control," *IEEE/ACM Trans. Netw.*, vol. 8, no. 5, pp. 556–567, 2000.
- [37] D. Noh and T. Abdelzaher, "Efficient flow-control algorithm cooperating with energy allocation scheme for solar-powered WSNs," *Wireless Comm. and Mobile Comput.*, 2010.
- [38] D. Palomar and M. Chiang, "A tutorial on decomposition methods for network utility maximization," *IEEE J. Sel. Areas Commun.*, vol. 24, no. 8, pp. 1439–1451, 2006.
- [39] J. Paradiso and T. Starner, "Energy scavenging for mobile and wireless electronics," *IEEE Pervasive Comput.*, vol. 4, no. 1, pp. 18–27, 2005.
- [40] V. Raghunathan, A. Kansal, J. Hsu, J. Friedman, and M. Srivastava, "Design considerations for solar energy harvesting wireless embedded systems," in *Proc. IEEE IPSN'05*, Apr. 2005.
- [41] J. Randall, *Designing Indoor Solar Products*, 1st ed. Wiley, 2005.
- [42] R. Rao, S. Vrudhula, and D. Rakhmatov, "Battery modeling for energy aware system design," *IEEE Computer*, vol. 36, no. 12, pp. 77–87, 2003.
- [43] S. Russel, *The Architecture of Light*. Conceptnine, 2008.
- [44] N. Sharma, J. J. Gummesson, D. Irwin, and P. Shenoy, "Cloudy computing: leveraging weather forecasts in energy harvesting sensor systems," in *Proc. IEEE SECON'10*, June 2010.
- [45] J. Taneja, J. Jeong, and D. Culler, "Design, modeling, and capacity planning for micro-solar power sensor networks," in *Proc. IEEE IPSN'08*, Apr. 2008.
- [46] C. Vigorito, D. Ganesan, and A. Barto, "Adaptive control of duty cycling in energy-harvesting wireless sensor networks," in *Proc. IEEE SECON'07*, June 2007.
- [47] D. Wentzloff, F. Lee, D. Daly, M. Bhardwaj, P. Mercier, and A. Chandrakasan, "Energy efficient pulsed-UWB CMOS circuits and systems," in *Proc. IEEE ICUWB'07*, Sept. 2007.
- [48] Y. Yang, L. Su, Y. Gao, and T. Abdelzaher, "SolarCode: utilizing erasure codes for reliable data delivery in solar-powered wireless sensor networks," in *Proc. IEEE INFOCOM'10 (mini-conference)*, Mar. 2010.
- [49] Y. Yang, L. Wang, D. K. Noh, H. K. Le, and T. F. Abdelzaher, "SolarStore: Enhancing data reliability in solar-powered storage-centric sensor networks," in *Proc. ACM MobiSys'09*, 2009.
- [50] K. Zeng, K. Ren, W. Lou, and P. J. Moran, "Energy aware efficient geographic routing in lossy wireless sensor networks with environmental energy supply," *Wirel. Netw.*, vol. 15, no. 1, pp. 39–51, 2009.
- [51] T. Zhu, Z. Zhong, Y. Gu, T. He, and Z.-L. Zhang, "Leakage-Aware Energy Synchronization for Wireless Sensor Networks," in *Proc. ACM MobiSys'09*, 2009.

I. APPENDIX: PROOF OF OBSERVATION 1

Lemma 2: Let $U(s)$ in *TFU-LIN* be a twice continuously differentiable concave function. Then the solution for *TFLA-LIN* and the solution for *TFU-LIN* are the same.

Proof:

First notice the following facts.

Fact 1: The constraint sets of both problems are the same, thus a feasible vector to one problem will also be a feasible vector to the other.

Fact 2: The nature of constraint set and the utility functions implies that any ϵ -decrease to one of the components of either solution yields at most total ϵ -increase to the rest of the components.

Fact 3: Let $y \leq x$ and let f be a twice continuously differentiable concave function. Then for every $\epsilon > 0$ we have $f(x + \epsilon) + f(y - \epsilon) \leq f(x) + f(y)$.

Proof: Since f is concave and twice differentiable we know that $f'' < 0$ and f' is a decreasing function. Using Taylor expansion we obtain,

$$\begin{aligned} f(x + \epsilon) + f(y - \epsilon) \\ = f(x) + f'(x)\epsilon + f(y) + f'(y)(-\epsilon) + o(\epsilon^2) \end{aligned}$$

$f'' < 0$ therefore,

$$\leq f(x) + f(y) + \epsilon(f'(x) - f'(y)) \leq f(x) + f(y),$$

since f' is decreasing. ■

Let \bar{s} be the optimal solution to the *TFLA-LIN* problem. We want to show that it is also the solution to the *TFU-LIN* problem. Assume not, that is there exists a vector \tilde{s} , $\tilde{s} \neq \bar{s}$, which is the optimal solution for the *TFU-LIN* problem. For simplicity, assume that the two vectors differ from each other only by two components (the following arguments also apply if they differ by more than two components). Therefore, by Fact 2 there exist j, k and $\epsilon > 0$, such that, $\tilde{s}(j) = \bar{s}(j) + \epsilon$ and $\tilde{s}(k) = \bar{s}(k) - \epsilon$. Note that $\tilde{s}(j) \geq \bar{s}(k)$, otherwise we would

get a contradiction for \bar{s} being the solution to the *TFLA-LIN* problem. Therefore, from the uniqueness of the solution,

$$\begin{aligned} U(\bar{s}(j)) + U(\bar{s}(k)) &< U(\tilde{s}(j)) + U(\tilde{s}(k)) \\ &\leq U(\bar{s}(j)) + U(\bar{s}(k)) \end{aligned}$$

where the last inequality obtained by applying Fact 3. This contradicts the assumption that $\tilde{s} \neq \bar{s}$ and shows that the unique solution to the *TFLA-LIN* problem is also the solution to the *TFU-LIN* problem. Notice that this also shows the converse, that is, if \tilde{s} is the (unique) solution to the *TFU-LIN* problem, then it also the solution to the *TFLA-LIN* problem. Indeed, any ϵ -increase in one of \tilde{s} components can only come on the expense of “weaker” components (using Fact 3), which is exactly the characteristics of the solution of the *TFLA-LIN* problem. This completes the proof. ■

Remark 1: Notice that the $U_\alpha(\cdot)$ functions satisfy the conditions of the lemma for every $\alpha \geq 0$, and this shows that Observation 1 is indeed true.

II. APPENDIX: PROOF OF PROPOSITION 1

If the s^* -policy is feasible, constraints (3) – (7) reduce to the requirements that $s(i) \geq 0$ and $\sum_{i=1}^K s(i) \leq \sum_{i=1}^K \Gamma(i) + (B_1 - B_{K+1}) = K \cdot s^*$. Our goal is to prove that in this case the s^* -policy is the optimal solution for the *TFU-LIN* problem when using α -fair function in our objective, that is when we want to solve

$$\max_{s(i)} \bar{U} = \sum_{i=1}^K U_\alpha(s(i))$$

for $\alpha \geq 0$, in our feasible domain.

Below we first present the proof for $\alpha = 1$, $U_1(s) = \log(s)$. Then, we demonstrate how to extend it to an arbitrary choice of $\alpha \geq 0$.

Optimality of s^* policy for α -fair objective functions with $\alpha = 1$: Since $\lim_{s \rightarrow 0} \log(s) = -\infty$, in order to find the maximum it suffices to search for it in domains of the form

$$\begin{aligned} D_\epsilon &= \{s = (s(1), \dots, s(K)) : \\ &\epsilon \leq s(i) \forall i, \sum_{i=1}^K s(i) \leq \sum_{i=1}^K \Gamma(i) + (B_1 - B_{K+1})\} \end{aligned}$$

for $\epsilon > 0$ small as we wish.

\bar{U} is a smooth function over D_ϵ , D_ϵ is a compact domain, therefore the maximum of the function \bar{U} is attained. $\nabla \bar{U} \neq 0$, hence the maximum lies on the boundary. Analysis of the behavior of \bar{U} on the boundary (using Lagrange multipliers, for example) yields a set of extreme points of the form

$$\left(\underbrace{\epsilon, \dots, \epsilon}_i, \dots, \underbrace{\frac{\sum_{i=1}^K \Gamma(i) + (B_1 - B_{K+1})}{K-i}, \dots, \frac{\sum_{i=1}^K \Gamma(i) + (B_1 - B_{K+1})}{K-i}}_{K-i} \right)$$

for $0 \leq i \leq K-1$, including all permutations. Since ϵ close to zero, the maximum point is the point of the above form, where none of its coordinates is equal to ϵ . There is only one point that fits this demand, when $i = 0$, and this is exactly the s^* -policy.

Optimality of s^* policy for other choices of α in α -fair objective functions: Following exactly the same arguments, one can prove the optimality of the s^* -policy for the case when using $U_\alpha(\cdot)$ function for $\alpha > 1$. For choice of α , $0 \leq \alpha < 1$, the proof is similar to the one that is given above, but there is no need for defining D_ϵ domains.

III. APPENDIX: SOLVING P-TFLA

Similarly to the single-node case, the *P-TFLA* can be solved as a set of *linear programming problems*. We define A_{fix}^u and A_{fix}^v to be the set of slot indexes for nodes u and v for which the lexicographically maximal data rates r_u and r_v have been determined. Starting with $A_{fix}^u = \emptyset$, $A_{fix}^v = \emptyset$, we solve the linear sub-problem:

$$\tilde{r} = \max \min \{r_u(i), r_v(j)\} \text{ over all } i \notin A_{fix}^u, j \notin A_{fix}^v \quad (21)$$

$$\text{s.t.:} \quad (11), (12)$$

$$u, v : \text{constraints (3) – (7)}$$

where on each iteration at least one value of $r_u(i)$ or $r_v(i)$ gets determined. The **Progressive Filling Algorithm for Link Based Communications (PFA-L)** (algorithm 2) can be used to solve problem *P-TFLA* without requiring solving linear problems.

IV. APPENDIX: SOLVING THE SRD

Here we provide an example of a solution for problem (14) for the objective function $U(r) = \log(r)$. Recall that for a given slot i , the problem to be solved is:

$$\max_{r_u(i), r_v(i)} U(r_u(i)) + U(r_v(i)) \quad (22)$$

$$\text{s.t.:} \quad \begin{aligned} c_{tx} \cdot r_u(i) + c_{rx} \cdot r_v(i) &\leq s_u(i) \\ c_{tx} \cdot r_v(i) + c_{rx} \cdot r_u(i) &\leq s_v(i) \end{aligned}$$

Since we are dealing with a given slot i , we drop it from the formulation. Without loss of generality, we may assume that $s_v = \gamma s_u$ for some $0 \leq \gamma \leq 1$. The gradient of our objective function is never zero, therefore the maximum is attained on the boundary. The boundary of the feasible set is a polygon. Since the log is a monotonic increasing function, it suffices to look for the maximum on the straight lines $c_{tx} r_u + c_{rx} r_v = s_u$ and $c_{tx} r_v + c_{rx} r_u = s_v$ within the feasible domain. If the intersection point of the two lines is within the feasible domain, we need to treat it as a possible point for the maximum, due to the lack of smoothness of the boundary there. The actual points of the solution depend on the relationship between c_{tx} and c_{rx} . Below, three cases are considered: where transmission is more expensive than

Algorithm 2

```

 $A_{fix}^u \leftarrow \emptyset; A_{fix}^v \leftarrow \emptyset; r_u(i), r_v(i) \leftarrow 0 \forall i;$ 
while  $A_{fix}^u \neq \emptyset, A_{fix}^v \neq \emptyset$ 
  for  $i = 1; i \leq K; i ++;$  do
    if  $i \in A_{fix}^u$  then
       $\tilde{r}_u \leftarrow r_u; \tilde{r}_u(i) \leftarrow \tilde{r}_u(i) + \epsilon;$ 
       $valid \leftarrow \text{check\_validity}(\tilde{r}_u, r_v);$ 
      if  $valid == \text{TRUE}$  then  $r_u(i) \leftarrow \tilde{r}_u(i);$ 
      else  $A_{fix}^u := A_{fix}^u \cup i;$ 
    if  $i \in A_{fix}^v$  then
       $\tilde{r}_v \leftarrow r_v; \tilde{r}_v(i) \leftarrow \tilde{r}_v(i) + \epsilon;$ 
       $valid \leftarrow \text{check\_validity}(r_u, \tilde{r}_v);$ 
      if  $valid == \text{TRUE}$  then  $r_v(i) \leftarrow \tilde{r}_v(i);$ 
      else  $A_{fix}^v := A_{fix}^v \cup i;$ 
function check_validity( $r_u, r_v$ ):
   $B_u(i) \leftarrow 0 \forall i; B_u(1) \leftarrow B_{1,u};$ 
   $B_v(i) \leftarrow 0 \forall i; B_v(1) \leftarrow B_{1,v}; valid \leftarrow \text{TRUE};$ 
  for  $i = 2; i \leq K; i ++;$  do
     $s_u(i) \leftarrow c_{tx}r_u(i) + c_{rx}r_v(i);$ 
     $s_v(i) \leftarrow c_{tx}r_v(i) + c_{rx}r_u(i);$ 
     $B_u(i) \leftarrow \min(C_u, B_u(i-1) + q(G_u(i-1), B_u(i-1)) - s_u(i-1));$ 
     $B_v(i) \leftarrow \min(C_v, B_v(i-1) + q(G_v(i-1), B_v(i-1)) - s_v(i-1));$ 
    if  $s_u(i) > B_u(i)$  then  $valid \leftarrow \text{FALSE};$ 
    if  $s_v(i) > B_v(i)$  then  $valid \leftarrow \text{FALSE};$ 
   $B_{f,u} \leftarrow B_u(K) + q(G_u(K), B_u(K)) - s_u(K);$ 
   $B_{f,v} \leftarrow B_v(K) + q(G_v(K), B_v(K)) - s_v(K);$ 
  if  $B_{K+1,u} < B_{f,u}$  then  $valid \leftarrow \text{FALSE}$ 
  if  $B_{K+1,v} < B_{f,v}$  then  $valid \leftarrow \text{FALSE}$ 
  return  $valid$ 

```

reception, when reception is more expensive than transmission [21], and when they are equal to each other.

Case 1: $c_{tx} = \beta c_{rx}$ for some $\beta > 1$.

If $\frac{1}{\beta} < \gamma \leq 1$, the maximum point is either (23) or (24):

$$\{r_u, r_v\} = \left\{ \frac{\beta - \gamma}{\beta^2 - 1} \cdot \frac{s_u}{c_{tx}}, \frac{\gamma\beta - 1}{\beta^2 - 1} \cdot \frac{s_u}{c_{tx}} \right\} \quad (23)$$

$$\{r_u, r_v\} = \left\{ \frac{s_v}{2c_{tx}}, \frac{s_v}{2c_{tx}} \right\} \quad (24)$$

We need to check both points if $\gamma < \frac{2\beta}{\beta^2+1}$. Otherwise the solution is at point (23). If $0 \leq \gamma \leq \frac{1}{\beta}$, the maximum point is (24).

Case 2: $c_{rx} = \tilde{\beta}c_{tx}$ for some $\tilde{\beta} > 1$:

If $\frac{1}{\tilde{\beta}} < \gamma \leq 1$, the maximum point is either (25) or (26):

$$\{r_u, r_v\} = \left\{ \frac{\gamma\tilde{\beta} - 1}{\tilde{\beta}^2 - 1} \cdot \frac{s_u}{c_{tx}}, \frac{\tilde{\beta} - \gamma}{\tilde{\beta}^2 - 1} \cdot \frac{s_u}{c_{tx}} \right\} \quad (25)$$

$$\{r_u, r_v\} = \left\{ \frac{s_v}{2c_{tx}}, \frac{s_v}{2c_{tx}} \right\} \quad (26)$$

If $\gamma < \frac{2\tilde{\beta}}{\tilde{\beta}^2+1}$, we need to check both points (25) and (26). Otherwise, the solution is point (25). If $0 \leq \gamma \leq \frac{1}{\tilde{\beta}}$, the maximum point is (26).

Case 3: $c_{tx} = c_{rx}$ The solution is:

$$\{r_u, r_v\} = \left\{ \frac{s_v}{2c_{tx}}, \frac{s_v}{2c_{tx}} \right\} \quad (27)$$

Thus for the objective function $U(r) = \log(r)$, the solution to SRD can be calculated algebraically. The algebraic solutions for other α -fair objective functions (i.e, $U(r) = \log(1+r)$, $U(r) = \sqrt{r}$) can be found similarly to the above.

V. APPENDIX: POLICY IMPROVEMENT ALGORITHM APPLIED TO THE SRD

A policy R_k is a collection of spending rates $s_{R_k}(B)$ for $B \in \{0, 1, \dots, C\}$. We denote by $p_{B, \tilde{B}}(s_{R_k}(B))$ the probability to transition from state B to state \tilde{B} when spending s in state B , under policy R_k . Given $s_{R_k}(B)$, these *state transition probabilities* can be easily calculated from the characteristics of random variable G (random variable samples $[g_1, \dots, g_M]$ with corresponding probabilities $[p_1, \dots, p_M]$) and the storage characteristics $q(G, B)$.

Policy Improvement Algorithm (PIA) [25] works as follows:

- 1) Choose an arbitrary spending policy R . We use the following *linear policy* R : $s_R(B) \leftarrow g_M \cdot B/C$.
- 2) $k \leftarrow 1$.
- 3) Solve the system of equation assembled by considering equation (28) for $B \in \{0, \dots, C\}$:

$$g(R_k) = U(s_{R_k}(B)) + \sum_{\tilde{B}=0}^C p_{B, \tilde{B}}(s_{R_k}(B)) \cdot v_{\tilde{B}}(R_k) - v_B(R_k) \quad (28)$$

where $v_C \leftarrow 0$, and $v_0, v_1, v_2, \dots, v_{C-1}$ and $g(R_k)$ as unknowns.

- 4) For each state B :

$$\max_{s(B)} U(s_{R_k}(B)) + \sum_{\tilde{B}=0}^C p_{B, \tilde{B}}(s_{R_k}(B)) v_{\tilde{B}}(R_k) - v_B(R_k) \quad (29)$$

The resulting set of $s(B)$ values form the new policy R_{k+1} .

- 5) $k \leftarrow k + 1$.
- 6) Repeat 3), 4), 5) until policies converge.

For linear storage, the *PIA* generally runs faster than dynamic programming, and generally converges in a few iterations. On every iteration the *PIA* requires solving a system of $|B| + 1$ linear equations. Since the result of the *PIA* calculation is a long-term policy, it does not have to be frequently recomputed.